

Layer formation in horizontally forced stratified turbulence: connecting exact coherent structures to linear instabilities

Dan Lucas^{1†} C. P. Caulfield^{2,1} & Richard R. Kerswell³

¹Department of Applied Mathematics & Theoretical Physics, University of Cambridge, Centre for Mathematical Sciences, Wilberforce Road, Cambridge, CB3 0WA, UK

²BP Institute, University of Cambridge, Madingley Rise, Madingley Road, Cambridge, CB3 0EZ, UK

³School of Mathematics, University of Bristol, University Walk, Bristol, BS8 1TW, UK.

(Received xx; revised xx; accepted xx)

We consider turbulence in a stratified ‘Kolmogorov’ flow, driven by horizontal shear in the form of sinusoidal body forcing in the presence of an imposed background linear stable stratification in the third direction. This flow configuration allows the controlled investigation of the formation of coherent structures, which here organise the flow into horizontal layers by inclining the background shear as the strength of the stratification is increased. By numerically converging exact steady states from chaotic direct numerical simulations, we show, for the first time, a robust connection between linear theory predicting instabilities from infinitesimal perturbations to the robust finite amplitude nonlinear layered state observed in the turbulence. We investigate how the observed vertical length scales are related to the primary linear instabilities and compare to previously considered examples of shear instability leading to layer formation in other horizontally sheared flows (Deloncle *et al. J. Fluid Mech.*, 2007 vol. 570, pp. 297-305 Billant & Chomaz *J. Fluid Mech.* 2000 vol. 419, pp. 65-91.)

1. Introduction

Laboratory experiments, numerical simulations and even field measurements of turbulent flows which are strongly stably stratified are regularly observed to exhibit spontaneous layering where the density field is organised into relatively deep, relatively well-mixed regions or ‘layers’ separated by relatively thin ‘interfaces’ with enhanced density gradients (Park *et al.* 1994; Holford & Linden 1999^{a,b}; Oglethorpe *et al.* 2013; Thorpe 2016; Falder *et al.* 2016; Leclercq *et al.* 2016). Scaling analyses (Billant & Chomaz 2001; Lindborg 2006) have provided some theoretical basis for the expected behaviour of vertical scales relative to the basic parameters involved in the distinguished asymptotic limit of extremely ‘strong’ stratification and intense turbulence. At its heart this scaling has the central idea that sufficiently strong stratification (definable in a precise fashion) inevitably introduces anisotropy into the velocity field: vertical velocities are suppressed by the buoyancy force compared to horizontal velocity components, thus leading to pancake-like layering, with characteristic turbulent regions having much larger greater horizontal extent l_h than vertical extent l_v . Indeed, following Falder *et al.* (2016), we refer to this regime as the ‘layered anisotropic stratified turbulence’ (LAST) regime.

Even in a purely one-dimensional model, where there is no characteristic horizontal scale l_h , and so the LAST regime is formally not possible, the hypothesis that sufficiently

† Email address for correspondence: dl549@cam.ac.uk

strong stratification suppresses vertical motions can lead to a prediction of layering in the density field. Specifically, if the vertical velocity is suppressed, it is at least plausible that some appropriately averaged vertical (turbulent) buoyancy flux should decrease with sufficiently strong stratification. As originally argued by Phillips (1972), if there is a range of stratifications for which the vertical (turbulent) buoyancy flux decreases with increasing stratification, local perturbations in density gradient will tend to be intensified rather than smoothed out by turbulent mixing, suggesting that uniform density gradients are ‘unstable’, in that they are prone to developing a layer-interface structure (see Park *et al.* (1994) for a clear discussion). Although in its simplest formulation (where for sufficiently strong stratification the buoyancy flux decreases monotonically with stratification) this Phillips mechanism is ill-posed, corresponding essentially to an ‘anti-diffusive’ problem, various regularisation mechanisms to limit the ‘sharpness’ of the interfacial density gradients have been proposed. For example, Barenblatt *et al.* (1993) demonstrated that the underlying problem could become well-posed if there was a time-lag between the turbulence and the mixing irreversibly modifying the density distribution, and there is at least some evidence that just such a time-lag exists in transient turbulent mixing driven by shear instabilities (Mashayek *et al.* 2013). Alternatively, Balmforth *et al.* (1998) proposed that the relationship between buoyancy flux and stratification should be ‘N-shaped’, with a return to an increase in buoyancy flux with increasing and sufficiently large stratification. Indeed, the possibly non-monotonic dependence of irreversible buoyancy flux on external parameters is a very active area of research controversy (see e.g. Venayagamoorthy & Koseff (2016); Venaille *et al.* (2016); Maffioli *et al.* (2016)). Importantly however, the fundamental physical mechanisms leading to either the formation or the maintenance of layered density distributions is still quite open.

One highly promising possible mechanism is suggested by the linear instability of a vortex dipole in a stratified environment, known as the zig-zag instability (Billant & Chomaz 2000*b*). The **linear** theory of the instability provides a scaling for layer depth which has been confirmed **at finite amplitude** numerically and experimentally (Billant & Chomaz 2000*a,b,c*; Deloncle *et al.* 2008; Waite & Smolarkiewicz 2008; Augier *et al.* 2015) resulting in the zig-zag instability being a popular explanation for the observation of layers (Thorpe 2016). A significant question is therefore how generic is a ‘zig-zag’ mechanism? Specifically, given other horizontally varying base flows, constituting other, less precisely organised distributions of vertical vorticity, do analogous linear instabilities exist to provide vertical structure? In addition, is it possible to make a more robust connection between such a linear stability mechanism and a highly nonlinear, yet identifiable sustained turbulent state? For example Deloncle *et al.* (2008) did not observe nonlinear saturation in their simulations of the zig-zag instability of counter-rotating vortex pairs.

Here we consider the case when forcing provides a horizontal shear which resembles in at least some respects the case of (vertically) stratified Taylor-Couette flow considered by Oglethorpe *et al.* (2013); Leclercq *et al.* (2016) (minus rotation and curvature, but where both non-monotonic buoyancy flux with stratification and spontaneous layer formation is known to occur) and the vertically invariant base flows of Billant & Chomaz (2000*b*) and Deloncle *et al.* (2007). We are further motivated by the results of Basak & Sarkar (2006) who considered the freely decaying case of a horizontal shear layer in a stratified environment. They found that, compared to its vertically sheared counterpart, the flow exhibits more intense turbulence as the stratification does not penalise the initial two-dimensional linear instability of the shear layer. They also observed ‘dislocated pancake vortices’, in that the flow exhibits vertical structure, but low vertical velocity, at strong stratification, precisely as postulated for the Billant & Chomaz scaling and the Phillips

mechanism. Of interest here is whether a **sustained** horizontal shear gives rise to sustained density layering and how the flow is organised in such a situation. Of course, it is important to remember that horizontal shear also has great relevance to oceanic flows, where zonal jets provide horizontal shear but are also observed to develop vertical structure in the form of ‘stacked jets’ (Eden & Dengler 2008; Hua *et al.* 1997).

We force our model system via a sinusoidal body-forcing term, leading to what is known as Kolmogorov flow (Arnold & Meshalkin 1960), a flow known to support a rich array of spatiotemporal behaviour (Lucas & Kerswell 2014). Stratified Kolmogorov flow has also been studied in two dimensions when the shear is oriented vertically (Balmforth & Young (2002, 2005) who consider the linear instabilities, weakly nonlinear theory and direct numerical simulation of the flow). Here some layering connected to a stratified conductive instability is observed when the Prandtl number (i.e. the ratio of the diffusivity of the density field to the kinematic viscosity) is small. The three-dimensional extension of this work was recently considered by Garaud *et al.* (2015) who, motivated by astrophysical systems, consider the low Péclet number case. They investigate the limits of linear and energy stability and find that strong enough stratification will eventually suppress all instabilities.

Our approach here is to make use of recent developments in (unstratified) shear flow transition where unstable exact coherent structures (ECSs) have been computed and shown to be responsible for organising the transition to and sustenance of turbulence (Kawahara & Kida 2001; van Veen *et al.* 2006; Kerswell & Tutty 2007; Viswanath 2007; Cvitanović & Gibson 2010; Kreilos & Eckhardt 2012; Kawahara *et al.* 2012; Willis & Short 2015). This is made possible by employing a high dimensional Newton-GMRES-hookstep algorithm which is able to converge *unstable* steady and time-periodic solutions efficiently from guesses taken from a chaotic simulation (Chandler & Kerswell 2013; Lucas & Kerswell 2015).

This study forms the first comprehensive investigation of layer formation in horizontally *driven* simulations and the role of nonlinear ECSs in creating such layers. Such a simple basic flow and periodicity in all directions makes the system an efficient setting for the so-called ‘dynamical systems approach’. Fundamentally, our philosophy is to focus on ‘structures not statistics’, as we aim to identify the characteristic, inherently nonlinear structures associated with (robust) layer formation in a stratified flow subjected to horizontal shear.

The rest of the paper is organised as follows. In section 2, we present the formulation of the flow which we are considering. In section 3, we describe the results of our nonlinear direct numerical simulations, where we do indeed observe the development of layered structures. In section 4 we present the results of a linear stability analysis of our flows, showing that there is a clear connection between the linear instabilities of the horizontally sheared stratified Kolmogorov flow and the linear three-dimensional instability studied by Deloncle *et al.* (2007). We then identify some exact coherent structures in section 5 and demonstrate that they can be connected both to the observed zig-zag structures in the nonlinear simulations and the predicted linear instabilities. We discuss our results and draw conclusions in section 6.

2. Formulation

We begin by considering the following version of the monochromatic body-forced, incompressible, Boussinesq equations

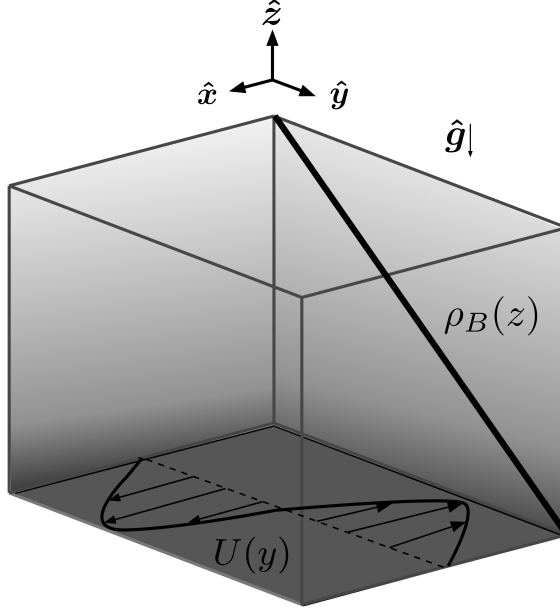


FIGURE 1. Schematic showing the base flow and the background stratification.

$$\frac{\partial \mathbf{u}^*}{\partial t^*} + \mathbf{u}^* \cdot \nabla^* \mathbf{u}^* + \frac{1}{\rho_0} \nabla^* p^* = \nu \Delta^* \mathbf{u}^* + \chi \sin(2\pi n y^*/L_y) \hat{\mathbf{x}} - \frac{\rho^* g}{\rho_0} \hat{\mathbf{g}}, \quad (2.1)$$

$$\frac{\partial \rho^*}{\partial t^*} + \mathbf{u}^* \cdot \nabla^* \rho^* + \mathbf{u}^* \cdot \nabla^* \rho_B = \kappa \Delta^* \rho^* \quad (2.2)$$

$$\nabla^* \cdot \mathbf{u}^* = 0 \quad (2.3)$$

$$(2.4)$$

where $\mathbf{u}^*(x, y, z, t) = u^* \hat{\mathbf{x}} + v^* \hat{\mathbf{y}} + w^* \hat{\mathbf{z}}$ is the three-dimensional velocity field, n is the forcing wavenumber, χ the forcing amplitude, ν is the kinematic viscosity, κ is the density diffusivity, p^* is the pressure, ρ_0 is an appropriate reference density and $\rho^*(x, y, z, t)$ the varying part of the density away from the background linear density profile $\rho_B = -\beta z$, i.e. $\rho_{\text{total}} = \rho_0 + \rho_B(z) + \rho^*(x, y, z, t)$. The unit vector $\hat{\mathbf{g}} = \hat{\mathbf{z}}$ orients the direction of gravity, which acts vertically downwards as shown in figure 1. We impose periodic boundary conditions in all directions $(x, y, z) \in [0, L_x] \times [0, L_y] \times [0, L_z]$ on \mathbf{u}^* and ρ^* .

For simplicity we set $L_f = L_y = L_z$. The system is naturally non-dimensionalised using the characteristic length scale $L_f/2\pi$, characteristic time scale $\sqrt{L_f/2\pi\chi}$ and density gradient scale $\beta = -\nabla \rho_B \cdot \hat{\mathbf{g}}$ to give

$$\frac{\partial \mathbf{u}}{\partial t} + \mathbf{u} \cdot \nabla \mathbf{u} + \nabla p = \frac{1}{Re} \Delta \mathbf{u} + \sin(ny) \hat{\mathbf{x}} - B \rho \hat{\mathbf{g}}, \quad (2.5)$$

$$\frac{\partial \rho}{\partial t} + \mathbf{u} \cdot \nabla \rho = w + \frac{1}{RePr} \Delta \rho \quad (2.6)$$

$$\nabla \cdot \mathbf{u} = 0 \quad (2.7)$$

where we define the Reynolds number Re , a buoyancy parameter B , the Prandtl number

Pr and the aspect ratio of the domain α as

$$Re := \frac{\sqrt{\chi}}{\nu} \left(\frac{L_y}{2\pi} \right)^{3/2}, \quad B := \frac{g\beta L_y}{\rho_0 \chi 2\pi} = \frac{N_B^2 L_y}{2\pi \chi} = \frac{1}{4\pi^2 F_{hB}^2}, \quad Pr := \frac{\nu}{\kappa}, \quad \alpha = \frac{L_f}{L_x}. \quad (2.8)$$

where N_B is the (dimensional) buoyancy frequency associated with the background density field, and the characteristic velocity in this particular (background) definition of the horizontal Froude number $F_{hB} = U/(L_f N_B)$ has been constructed using the characteristic length scale divided by the characteristic time scale, exactly as in the definition of the Reynolds number.

It is important to note that the distinguished limit formally required of the scaling proposed by Billant & Chomaz (2001) is that the Reynolds number is large, (and so it is expected that the flow is turbulent) while an appropriate horizontal Froude number F_h is small such that $Re F_h^2$ is still large. For our flows, if we use this background definition of F_{hB} , these conditions correspond to both Re and (much more stringently) $Re/(4\pi^2 B)$ being large. However, as discussed for example in Portwood *et al.* (2016), there are two significant, inter-related issues which are of interest. First, in practice, it is important to know the limits of applicability of a formally asymptotic scaling, identifying the finite limits for the various parameters to be sufficiently large or small so that the predicted regime actually arises. Second, and related to this, there is of course a freedom (not least in terms of the selection of factors of 2π for example) in the specific form of the various characteristic length scales, and so comparison of specific delimiting numerical values of these non-dimensional parameters quoted in different studies must be done with care. As discussed in more detail by Portwood *et al.* (2016), parameters based on the internal properties of any ensuing turbulent flow are more straightforward to compare from one flow to another (or indeed from one sub-region of a flow to another) and so we will also consider alternative measures for the key scaling of the internal Froude number in terms of the internal properties of the turbulence.

The equations then are solved over the cuboid $[0, 2\pi/\alpha] \times [0, 2\pi]^2$. We define the diagnostics involved in the energetic budgets as

$$\mathcal{E} = \frac{1}{2} \langle |\mathbf{u}|^2 \rangle_V, \quad \mathcal{I} = \langle \mathbf{u} \cdot \mathbf{f} \rangle_V = \langle u \sin(ny) \rangle_V, \quad (2.9)$$

$$\mathcal{B} = \langle \mathbf{u} \cdot B\rho \hat{\mathbf{z}} \rangle_V = \langle wB\rho \rangle, \quad \mathcal{D} = \frac{1}{Re} \langle |\nabla \mathbf{u}|^2 \rangle_V, \quad \mathcal{D}_{lam} = \frac{Re}{2n^2}, \quad (2.10)$$

where \mathcal{E} is the total kinetic energy density, \mathcal{I} is the energy input by the forcing, \mathcal{B} is the buoyancy flux, and \mathcal{D} is the dissipation rate. \mathcal{D}_{lam} is the dissipation rate associated with the basic state

$$\mathbf{u}_{lam} = \frac{Re}{n^2} \sin(ny) \hat{\mathbf{x}}. \quad (2.11)$$

where the forcing and dissipation precisely balance and $\langle (\cdot) \rangle_V := \alpha \iiint (\cdot) dx dy dz / (2\pi)^3$ denotes a volume average. We consider only $n = 1$ throughout, i.e. the flow is forced with $\sin(y) \hat{\mathbf{x}}$ and denote a time average with an overbar, i.e. $\bar{(\cdot)} = [\int_0^T (\cdot) dt] / T$ where T is normally the full simulation time. Vorticity $\boldsymbol{\omega} = \nabla \times \mathbf{u}$ is used as the prognostic variable and direct numerical simulations (DNS) are performed using the fully dealiased (two-thirds rule) pseudospectral method with mixed fourth order Runge-Kutta and Crank-Nicholson timestepping implemented in CUDA to run on GPU cards. This code is a further extension of that used in Lucas & Kerswell (2016). Each simulation is run on one GPU card and due to memory limitations on the current generation of NVIDIA chips we are restricted to resolutions of $N_x = N_y = N_z = 256$. We initialise the flow

velocity field's Fourier components with uniform amplitudes and randomised phases in the range $2.5 \leq |\mathbf{k}| \leq 9.5$ such that the total entstrophy $\langle |\boldsymbol{\omega}|^2 \rangle_V = 1$ and leave the density field unperturbed initially i.e. $\rho = 0$. Spatial convergence is checked by comparing the Kolmogorov microscale $\eta = (Re^3 \mathcal{D})^{-1/4}$ with the smallest permitted scale in the system, i.e. the maximum wavenumber in simulation $k_{\max} = N_x/3 = 85$, in other words we ensure $k_{\max} \eta > 1$.

3. Direct numerical simulation

To determine the effect of stratification on this flow we begin by performing direct numerical simulations with various B at fixed $Re = 100$, $Pr = 1$, $n = 1$, $\alpha = 1$, integrating until $T = 100$. Figure 2 shows yz planes (at $x = \pi$) of $t = 50$ snapshots of ρ and u along with $\langle \bar{\rho} \rangle_x$ and $\langle \bar{u} \rangle_x$, i.e. streamwise averages of the mean (in time over the whole simulation). Immediately we recognise the emergence of coherent structures organising the flow. Most evident in the mean, but also noticeable in the snapshots, is an inclining of the background horizontal shear into characteristic chevron, or (rotated) ‘v’ shapes. Associated with this structure is the organisation of the density field into vertical layers, the number of layers (and associated v-shapes in u) increasing with B . As the stratification is increased, the mean flow becomes progressively more layered. The formation mechanism of these layers, and in particular their relationship to both linear instabilities and exact coherent structures, will be discussed in the subsequent sections.

3.1. Recurrent bursts

One important feature of the inclined shear, observed from the DNS and figure 2, is that the mean flow now has a component of vertical shear. We find that for simulations with large B (i.e. for $B \geq 50$) vertical shear instability (of Kelvin-Helmholtz (KH) type) is suppressed and density variations with respect to z remain small. Due to the body-forced nature of this flow, quiescent episodes, when the vertical shear instability is suppressed, are associated with a build up of energy in the mean flow as energy is continually and uniformly injected via the forcing. This results in highly intermittent turbulent bursts as the flow is accelerated until apparently a local gradient Richardson number criterion is overcome, KH shear instability is initiated, grows to finite amplitude, breaks down to disordered motion and then decays until the mean is regenerated once again by the forcing (in fact this is the generic behaviour observed when the forcing itself provides vertical shear, i.e. $\sin(nz)\hat{\mathbf{x}}$). The final row of figure 2 shows some turbulent remnant in the $T = 50$ snapshots with apparent shear instability on the vertical bands of u . Figure 4 shows the full three-dimensional streamwise velocity for four snapshots in time, spanning the burst of spatiotemporal turbulence around $t \simeq 80 - 90$ apparent in figure 3.

Defining an appropriate gradient Richardson number

$$Ri_G(y, z, t) = \frac{-B \left\langle \frac{\partial \rho_{tot}}{\partial z} \right\rangle_x}{\left\langle \left(\frac{\partial u_h}{\partial z} \right)^2 \right\rangle_x}, \quad (3.1)$$

where the subscript denotes averaging in the streamwise x -direction, we plot a time series of the volume average $\langle Ri_G \rangle_V$ and $y - z$ snapshots at various times for the $B = 50$ simulation in figure 5. We find that the suppression of shear instability occurs in two distinct classes of thin strips. One class (at an angle to the vertical) is aligned with the minimum of the vertical shear. The other class (close to horizontal) is associated with the maximum of the density gradient, as is apparent from the bottom right two

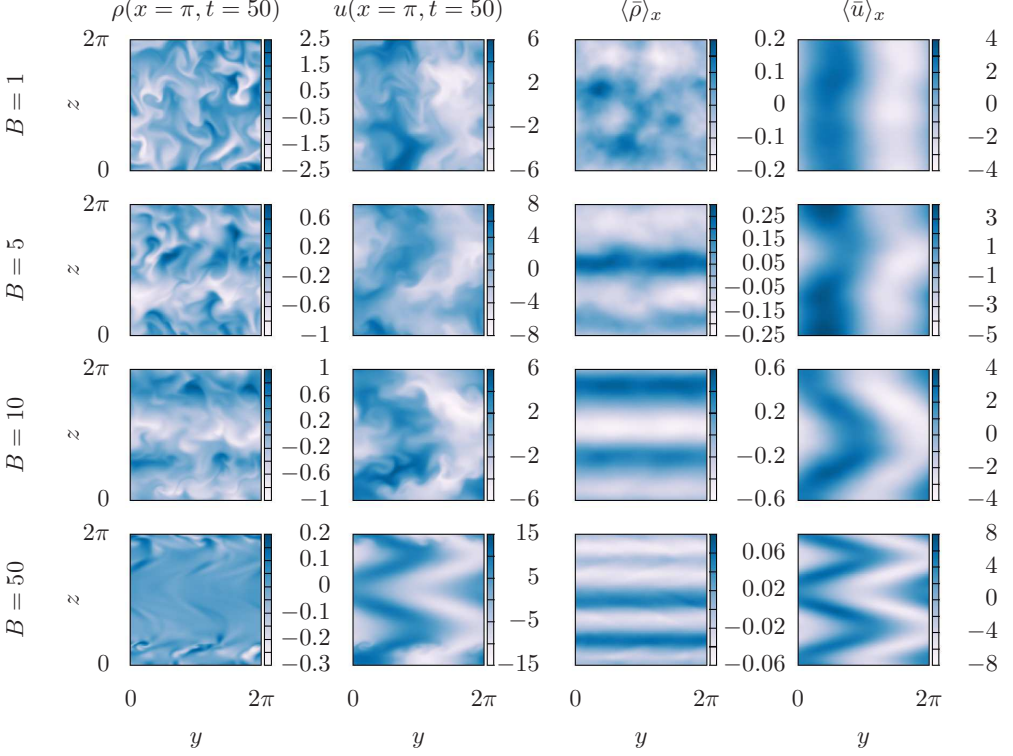


FIGURE 2. Snapshots in a yz mid-plane (at $x = \pi$ for simulations with $Re = 100$, $Pr = 1$, $n = 1$ and $\alpha = 1$) of ρ (first column) and u (second column) at $t = 50$. The third column shows $\langle \bar{\rho} \rangle_x$, while the fourth column shows $\langle \bar{u} \rangle_x$, i.e. x -average of the time-averaged (across the full $t \in [0, 100]$ interval) perturbation density and streamwise velocity. Rows are showing $B = 1, 5, 10, 50$ (simulations A1-A4 from table 1) from top to bottom. Notice the increase in vertical structure as B increases.

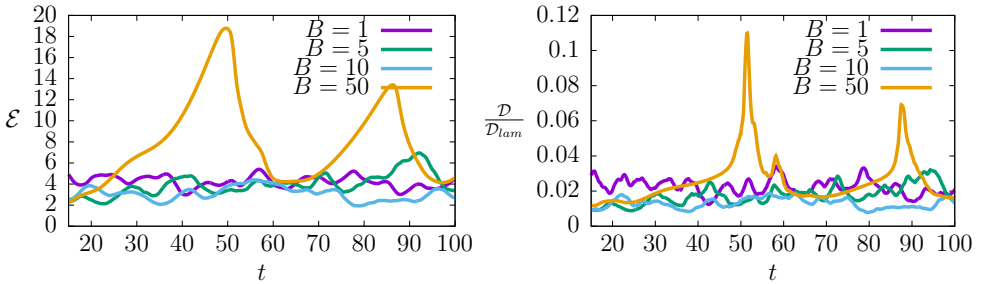


FIGURE 3. Time series of total kinetic energy density $\mathcal{E} = (1/2)\langle |u|^2 \rangle_V$ and volume-averaged scaled dissipation rate $\mathcal{D}/\mathcal{D}_{lam} = 2\langle |\nabla u|^2 \rangle_V / Re^2$, for simulations A1-A4 from table 1. Note the widely separated and yet intense recurrent bursts for simulation A4 with $B = 50$, and the lag between \mathcal{E} and the ensuing dissipation \mathcal{D} .

panels in figure 2. In other words the horizontal structures in figure 5 are caused by large density gradient in the numerator of Ri_G and the inclined structures are caused by minima of the shear in the denominator of Ri_G . This lattice structure of the two classes of strips effectively covers the entire flow domain, and eventually manages to stabilise the flow globally. Once the flow is accelerated again sufficiently we then observe instability

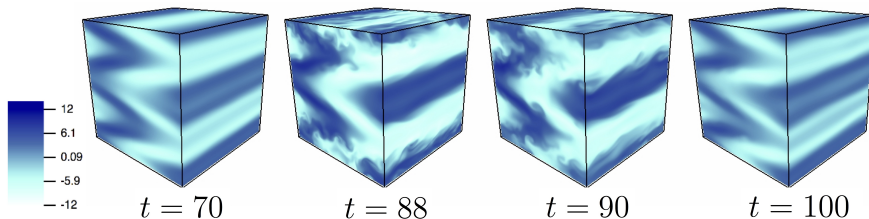


FIGURE 4. Three-dimensional snapshots of streamwise velocity u at times $t = 70, 88, 90, 100$ showing the burst of turbulence for simulation A4 as defined in table 1 with $Re = 100$, $B = 50$, $Pr = 1$, $\alpha = 1$.

nucleating in the regions of minimal Ri_G in the gaps of this lattice, as is apparent in the frames associated with $t = 88$ in figures 4 and 5. Overall, for this flow, the volume average of Ri_G reaches a maximum value of $Ri_G \approx 0.2$ during the stabilising period, but it is not clear whether there is any significance to this particular value.

From a dynamical systems point of view, one may consider these observed cycles to be similar to the type of homoclinic tangle studied to explain bursting in plane Couette flow by van Veen & Kawahara (2011). We appear to observe a close approach to a coherent structure and a return to it via a complex turbulent trajectory which wraps up the stable and unstable manifold of the underlying solution. Unfortunately, this particular feature of close approach and complex (near) return makes this flow quite challenging computationally. As is particularly apparent for simulation A4 as shown in figure 3, as the buoyancy parameter B is increased further (i.e. the background buoyancy frequency is increased relative to the horizontal shear forcing) the mean flow required to maintain turbulence becomes stronger with more intense small-scale dissipation, which requires both smaller timesteps to resolve individual bursts of rapidly varying dissipation, and also longer integrations to approach steady statistics and average out the increasingly long intermittent bursting time scale.

3.2. Throttling

To attempt to overcome the combined computational challenge of increasingly long times between increasingly intense intermittent bursts as B is increased, we employ a throttling method similar to that used by Chung & Matheou (2012) to modulate the forcing amplitude with the aim of maintaining a mean dissipation rate. Therefore, we allow the forcing term in equation (2.5) to have a time varying amplitude, i.e.

$$\mathbf{f} = \chi(t) \sin(ny) \hat{\mathbf{x}}. \quad (3.2)$$

We then adjust $\chi(t)$ based on the instantaneous kinetic energy budget, i.e.

$$\frac{d\mathcal{E}}{dt} = \mathcal{I} + \mathcal{B} - \mathcal{D} \quad (3.3)$$

where \mathcal{E} , \mathcal{I} , \mathcal{B} and \mathcal{D} are the total kinetic energy density, volume-averaged energy input, buoyancy flux and dissipation rate respectively, as defined in (2.9)-(2.10). Following Chung & Matheou (2012) we set a target dissipation rate \mathcal{D}_0 and seek $\frac{d\mathcal{E}}{dt} = 0$, i.e. statistically stationary kinetic energy, so that

$$\chi(t) = \frac{\mathcal{D}_0 - \mathcal{B}}{\langle u \sin(y) \rangle}. \quad (3.4)$$

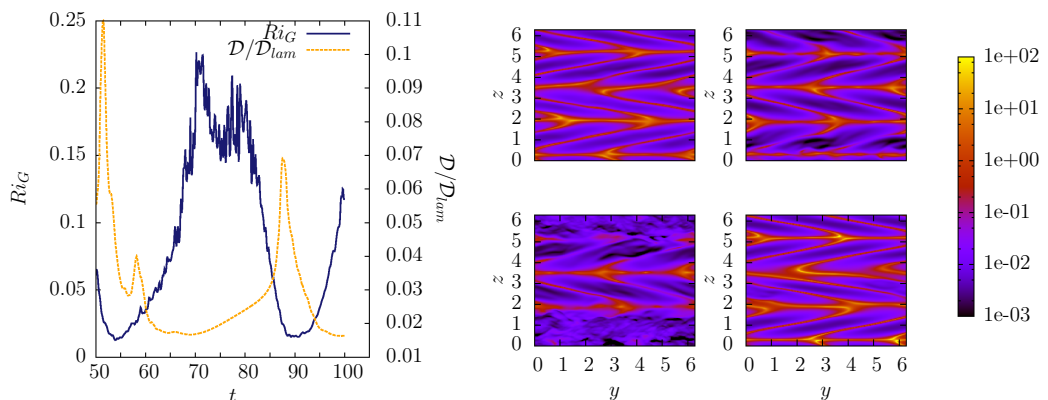


FIGURE 5. Left: Time dependence of the volume average of Ri_G and the scaled dissipation rate $\mathcal{D}/\mathcal{D}_{lam}$, showing the anti-correlation of turbulence intensity and gradient Richardson number; Right: Four snapshots of $Ri_G(y, z, t)$ at times $t = 70, 88, 90, 100$ simulation from A1 with $Re = 100$, $B = 50$, $Pr = 1$, $\alpha = 1$. Note the small values in the panels for $t = 88$ and $t = 90$ associated with the burst of turbulence near the top and bottom of the domain. By $t = 100$ the stabilising lattice of high values apparent in the panel for $t = 70$ has become re-established. Angled strips of high Ri_G are associated with minimal vertical shear, and horizontal strips of high Ri_G are associated with maximal density gradient.

In other words when $\mathcal{D} < \mathcal{D}_0$ the energy input is increased so that the total kinetic energy grows in time and when $\mathcal{D} > \mathcal{D}_0$ the flow is decelerated by reducing \mathcal{E} . Notice that the connections between the terms in equation (3.3) are inherently nonlinear and linked to the turbulent cascade: energy is input at the largest scale and is ultimately dissipated at much smaller scales. For this reason there is an inevitable lag between the adjustment of χ and the flow response. Furthermore, there are still undoubted computational challenges. To maintain adequate resolution at large external Re we cannot throttle with large \mathcal{D}_0 , although for statistical stationarity larger values of B require progressively larger \mathcal{D}_0 . For these reasons we chose the parameters in table 1 to maintain at least some semblance of a turbulent state at progressively stronger stratification.

Figure 6 shows equivalent yz -plane ρ and u snapshots and means to those shown in figure 2 for the throttled simulations D1, B3, C2 and C3 as listed in table 1, associated with larger values of the buoyancy parameter B . Figure 7 shows the time dependence of the kinetic energy density \mathcal{E} and scaled dissipation rate $\mathcal{D}/\mathcal{D}_0$. The throttling simulations exhibit approximately statistical stationarity near the target dissipation rate \mathcal{D} in contrast to the observed time-lagged bursting in both energy density and dissipation rate shown in figure 3 for the unthrottled simulation A4 with $B = 50$. Curiously, the throttling method doesn't reach the target dissipation rate \mathcal{D}_0 as closely as reported in Chung & Matheou (2012), with a systematic undershoot in the actually occurring dissipation rate \mathcal{D} . This difference is presumably due to the different nature of forcing between the two studies. In particular, Chung & Matheou (2012) enforce a specific background mean linear shear rather than a 'free' body force as in our simulations. In spite of this discrepancy, the method serves our purpose by providing a much more stationary flow at large B and the opportunity to investigate the trend in layer scale with B .

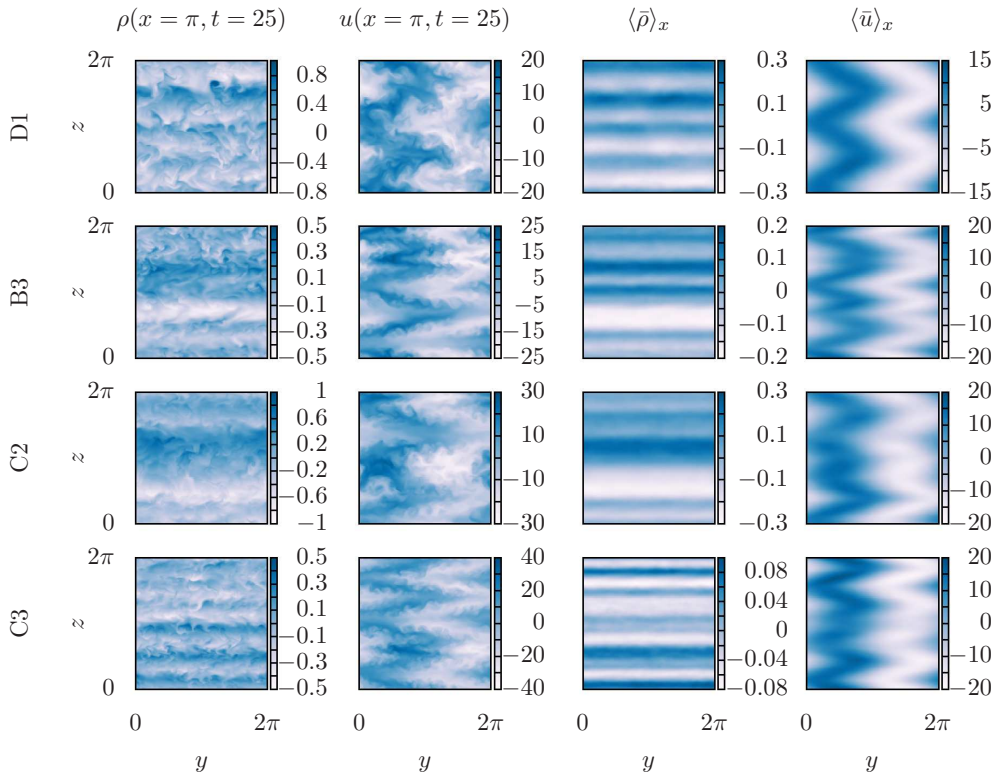


FIGURE 6. Snapshots in a yz mid-plane (at $x = \pi$) of ρ (first column) and u (second column) at $t = 25$. The third column shows $\langle \bar{\rho} \rangle_x$ and the fourth column shows $\langle \bar{u} \rangle_x$, i.e. the x -average of the time-averaged perturbation density and streamwise velocity. Time averages are over $t \in [0, T]$ as defined in table 1. Rows are showing data from simulations D1, B3, C2 and C3 (as defined in table 1) from top to bottom. Notice the increase in the number of layers as the buoyancy parameter B increases and the increasingly angled structure of the velocity field. All simulations have $Pr = 1$.

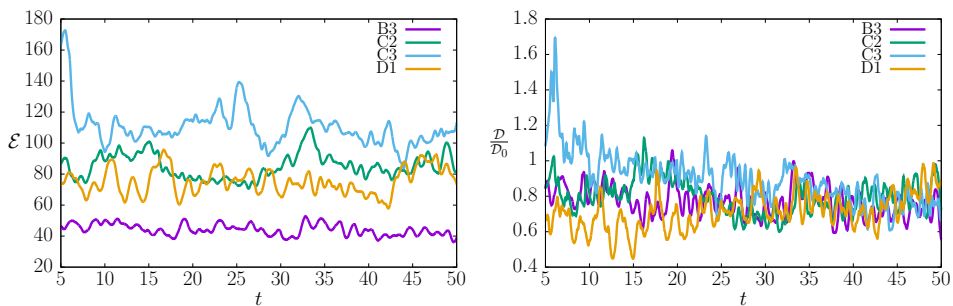


FIGURE 7. Time dependence of total kinetic energy $\mathcal{E} = (1/2)\langle |\mathbf{u}|^2 \rangle_V$ and scaled dissipation rate $\mathcal{D}/\mathcal{D}_0 = \langle |\nabla \mathbf{u}|^2 \rangle_V / Re^2$ for the various throttled simulations at large B whose fields are plotted in figure 6. Note that the dissipation fluctuates near, yet systematically below the target value \mathcal{D}_0 .

#	Re	B	D_0	U	ηk_{\max}	$l_{\bar{u}}$	l_o	Re_B	Re_λ	T
A1	100	1	-	1.3	2.6	2.5	1.05	110.9	56.6	100
A2	100	5	-	1.9	2.7	3.9	0.3	20.2	48.6	100
A3	100	10	-	1.7	3.0	3.5	0.15	6.8	41.8	100
A4	100	50	-	3.1	2.5	1.8	0.06	2.9	36.8	100
B1	100	50	50	7.3	1.03	4.5	0.37	94.9	178.7	50
B2	100	100	50	5.9	1.1	2.8	0.18	34.3	204.0	50
B3	100	200	50	6.9	1.08	2.1	0.12	19.3	159.8	50
C1	75	500	100	6.3	1.2	1.6	0.073	9.0	263.8	50
C2	75	1000	100	9.8	1.1	1.2	0.052	6.4	107.0	50
C3	75	2000	100	11.5	1.1	1.2	0.03	3.02	55.6	50
D1	50	500	100	7.8	1.6	1.7	0.079	7.1	54.3	50
D2	50	200	250	11.0	1.2	4.4	0.26	49.4	89.2	50
D3	50	500	250	10.8	1.3	2.8	0.11	14.9	114.2	50
D4	50	1000	250	10.7	1.3	2.4	0.071	7.9	121.2	50
D5	50	2000	250	12.1	1.2	1.4	0.046	4.7	131.2	50

TABLE 1. Imposed parameters and diagnostic simulation outputs for the four groups of simulations. Simulations in group A are unthrottled simulations, simulations in group B are throttled simulations with $Re = 100$, simulations in group C are throttled simulations with $Re = 75$, and simulations in group D are throttled simulations with $Re = 50$. The Kolmogorov microscale, within the chosen nondimensionalization is given by $\eta = (Re^3 \bar{D})^{-1/4}$ and is scaled by the maximum wavenumber allowable in the simulation $k_{\max} = N_x/3 = 85$. The nondimensional Ozmidov length scale $l_o = (\bar{D}/B^{3/2})^{1/2}$, the buoyancy Reynolds number $Re_B = \frac{\bar{D}Re}{B}$, a typical horizontal velocity scale given by $U = \langle |\bar{u}| \rangle_V$ and the Taylor microscale Reynolds number $Re_\lambda = \mathcal{E}_{\text{turb}} \sqrt{\frac{10Re}{D}}$ are also listed. Here we define $\mathcal{E}_{\text{turb}} = (1/2) \langle (\mathbf{u} - \bar{\mathbf{u}})^2 \rangle_V$ and overbars are always time averages over the full T window as specified in the table.

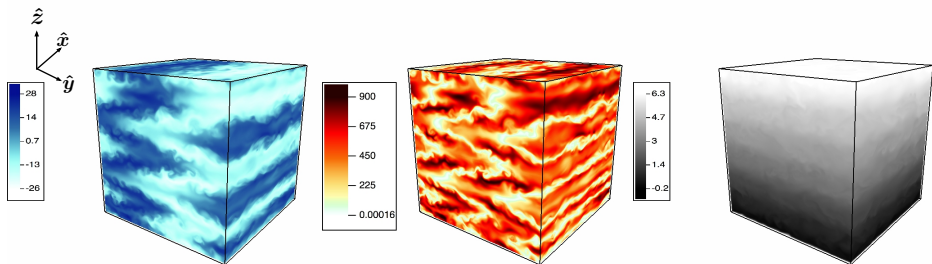


FIGURE 8. Three-dimensional rendering of, from left to left right: the streamwise velocity u ; the vertical shear $\frac{\partial u}{\partial z}$; and the total density field $\rho_B(z) + \rho$, for the throttled simulation C2 with parameters as listed in table 1. Note that regions of increased density gradient coincide once again with quiescent regions in u where the vertical shear is minimum.

3.3. Layer length scale

For the throttled simulations, it is now possible to observe smaller vertical length scales in the developing layered structures. The increased buoyancy flux due to the sustained turbulence in the inclined shear layers now spontaneously leads to sharpening interfaces separating relatively well-mixed ‘layers’. This spontaneous interface-layer formation can be most clearly seen in figure 9 (left panel) where profiles of the total density (including

the background linear component $\rho_B(z)$) are plotted. Figure 8 shows three-dimensional renderings of snapshots of the streamwise velocity, vertical shear $\frac{\partial u}{\partial z}$, and the total density field for the simulation C2 with $B = 1000$ and $\mathcal{D}_0 = 100$. It can be seen that gradients of density are approximately coincident with planes of small vertical shear of the underlying coherent structure, where vertical buoyancy flux is small, or more precisely away from regions of strong vertical shear.

A common characterisation of vertical length scales in stratified turbulent flows is the scaling proposed by Billant & Chomaz (2001) leading to the ‘layered anisotropic stratified turbulence’ (LAST) regime mentioned in the introduction. The characteristic vertical scale of the layers $l_v \sim U/N$ is commonly observed in simulation and experiments with U a typical velocity scale. As mentioned in the introduction, this scaling is strictly valid in a distinguished limit of small horizontal Froude number, $F_h = U/l_h N \rightarrow 0$, implying that $l_v \ll l_h$. Due not least to the periodicity of our computational domain, the formal requirement that $l_v \ll l_h$ cannot be satisfied in our computations (the layers typically span the full horizontal extent of the box). However, under the assumption that the dissipation rate has an inertial scaling (see Brethouwer *et al.* (2007)) the LAST regime may equivalently be associated with sufficiently large values of the buoyancy Reynolds number Re_B , defined as

$$Re_B = \frac{\epsilon}{\nu N_B^2} = \frac{\mathcal{D} Re}{B}. \quad (3.5)$$

As discussed in more detail in Portwood *et al.* (2016), Re_B is determined from the internal local characteristics of the turbulence (captured by the dissipation rate) relative to the joint stabilizing effects of the fluid’s viscosity and the background density gradient.

Although it is now becoming widely accepted (see for example Venayagamoorthy & Koseff (2016)) that Re_B alone cannot uniquely identify the properties of stratified turbulence driven by shear, the evidence is nevertheless strong that $Re_B \gtrsim O(10)$ is necessary for there to be any opportunity for the LAST regime to occur. As explained in detail by Brethouwer *et al.* (2007), this is due to the necessity for there to be large scale separations between three scales: the Kolmogorov microscale, $\eta = (Re^3 \mathcal{D})^{-1/4}$; the Ozmidov scale $l_O = (\mathcal{D}/B^{3/2})^{1/2}$ and some vertical scale of the layers l_v , which must be smaller than the vertical extent of the computational domain. The Ozmidov scale is the largest vertical scale which is largely unaffected by the background stratification, and so the ordering $\eta \ll l_O < l_v$ ensures that there is both an inertial range for the turbulent motions largely unaffected by the stratification, and a range of scales (between l_O and l_v) where the LAST regime occurs. Since by definition $Re_B = (l_O/\eta)^{4/3}$, Re_B must be sufficiently large for an inertial range to exist.

The formal accessibility of this hierarchy of length scales within our simulations is challenging. Due to the horizontal (periodic) boundary conditions, there is no natural way in which the actual **horizontal** extent of any layer can be identified. Furthermore, the observed vertical length scale of layers must be sufficiently small so that it can be measured within the vertical extent of the computational domain, yet still sufficiently large so that it is both resolved computationally and also larger than the Ozmidov length scale l_O . In turn, l_O must still be sufficiently large so that there is separation between it and the Kolmogorov microscale, which, for the entire simulation to be adequately resolved, must be at worst of the same order as the smallest scale of the simulation. These various length scales are listed in table 1. It is important to appreciate that, principally due to resolution constraints, several of the simulations, particularly when B is large, have values of Re_B which are too small for the flow to be strictly in the LAST regime. In particular, when

the dissipation rate \mathcal{D} in the definition (3.5) is taken to be the time-average of the actual (in general time-varying) volume-averaged dissipation rate within our simulations.

However, it is still of interest to investigate whether the spontaneous layers observed here are consistent with the scaling ideas at the heart of this proposed regime, even if the relevant parameters are not in the formally necessary self-consistent asymptotic scale separation. We choose to define an appropriate vertical ‘layer’ length scale $l_{\bar{u}}$ for the layers as

$$l_{\bar{u}} = \frac{2\pi \int \hat{u} dk_z}{\int k_z \hat{u} dk_z}, \quad (3.6)$$

where \hat{u} is the Fourier transform of the horizontally and temporally averaged ($t \in [0, T]$) streamwise velocity $\langle \bar{u} \rangle_{x,y}$. For the LAST regime as discussed above, the layer length scale should scale with the ratio of an appropriate large scale or background horizontal velocity scale U and the (dimensionless) buoyancy frequency $N_B = \sqrt{B}$ from (2.8). An appropriate choice for the velocity scale U is the volume and time-averaged absolute streamwise velocity $U = \langle |\bar{u}| \rangle_V$. Figure 9 shows $l_{\bar{u}}$ plotted against U/N_B . We find that for small U/N_B $l_{\bar{u}}$ approaches a linear trend, and is much more scattered as U/N_B reaches larger values, though still largely following the asymptotic prediction of Billant & Chomaz (2001), which is formally expected to occur as $U/N_B \rightarrow 0$. Significantly, the scaling appears to be satisfied even for the flows with relatively small buoyancy Reynolds number (see table 1) associated with relatively large values of B and hence N_B , where the LAST regime scaling arguments are not strictly valid. As is shown from the least-squares fit, the **vertical** Froude number F_v , defined as

$$F_v = \frac{U}{N_B l_u} \simeq 0.78 = \mathcal{O}(1), \quad (3.7)$$

consistently with the scaling regime of Billant & Chomaz (2001).

It should also be noted that similar estimates of layer depth could be constructed using the density field. However, due to the strong spatiotemporal intermittency at large B the trend to small U/N_B is harder to observe in the density field, since measurable layering of density requires sustained buoyancy fluxes and mixing, which are challenging to resolve. At higher resolutions where turbulence can be maintained with larger target dissipation rates at larger B , it is perfectly reasonable to expect that robust layering of the density field obeying the U/N_B scaling will be more straightforward to observe, as is strongly suggested in figure 8. A key question we now consider is how these layers form.

4. Linear stability analysis

There appears to be at least qualitative similarity between the streamwise velocity structure observed in our forced flows and the streamwise velocity eigenstructure at onset of the now classic ‘zig-zag’ instability mechanism of Billant & Chomaz (2000*a,b,c*). Since this class of instability is also often invoked as the precursor to layer formation (see e.g. Thorpe (2016)), it seems appropriate to investigate the linear stability properties of the flows we are considering, in particular to identify whether they are prone to instabilities which may be identified as being of ‘zig-zag’ type. For the case when the forcing scale and streamwise integral scale are the same (i.e. using our notation $\alpha = 1$ and $n = 1$), the unstratified three-dimensional Kolmogorov flow is known to undergo subcritical transition to turbulence with the base flow remaining linearly stable at all Re (Marchioro 1986; van Veen & Goto 2015). Any linear instability in this geometry is therefore due to the added physics provided by the statically stable stratification.

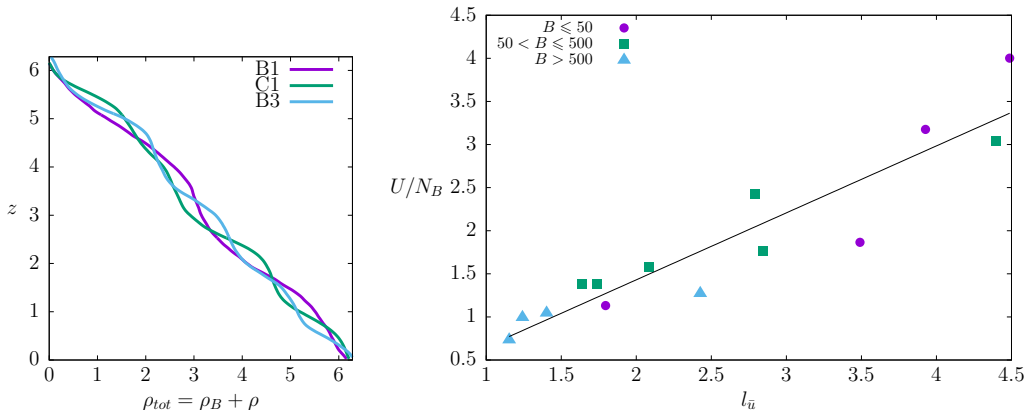


FIGURE 9. Left: profiles of total density $\rho_{\text{tot}} = \rho_B + \rho$ at $t = 50$, $x = y = \pi$ for cases B1, B3 and C1 from table 1. Right: Vertical lengthscale $l_{\bar{u}}$ as defined in (3.6) plotted against $U/N_B = \langle |\bar{u}| \rangle_V / \sqrt{B}$ for each DNS as in table 1. We find the scaling $l_v \sim U/N_B$ is recovered, particularly as $U/N_B \rightarrow 0$. A least squares linear fit is also plotted: $0.78l_{\bar{u}} - 0.12$.

The inviscid linear stability properties of a background horizontal tanh shear profile with linear background stratification was considered by Deloncle *et al.* (2007). They reported that, while two-dimensional (in the horizontal plane) homogeneous perturbations are the most unstable leading to instabilities of KH type associated with the inflection point in the background shear profile, new inherently three-dimensional stratified instabilities are present and can have comparable growth rates. The growth rates of the stratified instabilities are also observed to follow the self-similar scaling with respect to an appropriate horizontal Froude number as proposed by Billant & Chomaz (2001).

In the conventional fashion, we consider normal mode disturbances proportional to $\exp[i(k_x x + k_z z) + \sigma t]$, away from the base state $S_B = (U_B, \rho_B)$ defined by

$$U_B = \frac{Re}{n^2} \sin(ny) \hat{\mathbf{x}}, \quad \rho_B = -z, \quad (4.1)$$

and solve the ensuing eigenvalue problem for the linearised equations using the python NUMPY package, which is itself a front-end for LAPACK (van der Walt *et al.* 2011). We find very good agreement with the results of Deloncle *et al.* (2007) for the horizontal sinusoidal shear flow considered here provided $Re \gg 1$, which is a natural requirement as their analysis is inviscid. Figure 10 shows the variation with vertical wavenumber k_z of the maximal growth rate σ_m (across all streamwise wavenumbers, corresponding to $k_x = 0.59$) rescaled with Re (since $\sigma_m \sim Re$), plotted for a range of Re and B . Similarly to the results of Deloncle *et al.* (2007), we also find that two-dimensional disturbances (with $k_z = 0$) are most unstable and that the most unstable horizontal wavenumber k_x is independent of B . This is unsurprising, as this two-dimensional instability is once again of KH type associated with the inflection point in the background velocity shear. For further comparison with their results, it is necessary to define an appropriate horizontal Froude number for this stability problem. An appropriate velocity scale for comparison for these linear instabilities is the maximum magnitude of U_B i.e. Re/n^2 , (half the total velocity jump across the shear layer) while an appropriate length scale is (within our nondimensionalization) $1/n$, and so the stability horizontal Froude number F_{hs} may be defined as

$$F_{hs} = \frac{Re}{n\sqrt{B}}. \quad (4.2)$$

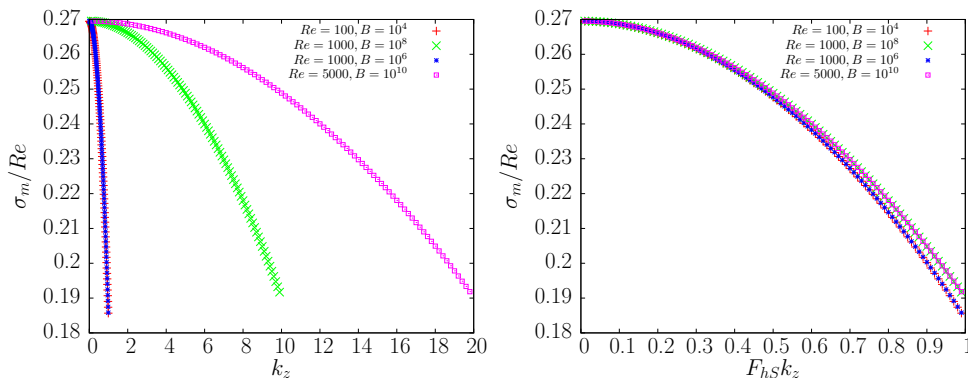


FIGURE 10. Variation of the maximum (across all horizontal wavenumbers, associated with $k_x = 0.59$) and scaled growth rate σ_m/Re with: vertical wavenumber k_z (left panel); and vertical wave number scaled with stability horizontal Froude number (as defined in (4.2) $F_{hs}k_z$ (right panel). Red pluses mark results for a flow with $Re = 100$, $B = 10^4$ ($F_{hs} = 1$), green crosses mark results for a flow with $Re = 1000$, $B = 10^8$ ($F_{hs} = 0.1$), red stars mark results for a flow with $Re = 1000$, $B = 10^6$ ($F_{hs} = 1$) and magenta squares mark results for a flow with $Re = 5000$, $B = 10^{10}$ ($F_{hs} = 0.05$).

As already noted, for all the calculations we presented here, we set $n = 1$. Replotting the growth rates against $F_{hs}k_z$ leads to a very good collapse of the curves for a wide range of stability horizontal Froude numbers $F_{hs} = (0.05, 0.1, 1)$ as shown in the right panel of figure 10, once again in pleasing agreement with Billant & Chomaz (2001) and Deloncle *et al.* (2007). In particular, see figure 4 in Deloncle *et al.* (2007) where an equivalent definition of horizontal Froude number (i.e. using the maximum magnitude of the velocity distribution and the scale of the shear layer) are used and the curves are extremely similar to those in figure 10; the shape of the shear profile serves only shift the growth rates slightly.

In the nonlinear direct numerical simulations, only horizontal wavenumbers $k_x = \frac{m}{\alpha}$ (where m is an integer) are admissible. Therefore, any linear instabilities must have $k_x \geq 1/\alpha$ to have any chance of occurring within our computational domain. In figure 11 (left panel) for flows with $B = 50$ we plot neutral curves of linear stability for various vertical wavenumbers k_z on the $Re - k_x$ plane. Although the unstratified long-wave instability is clearly evident for $k_z = 0$, the neutral curve asymptotes near $k_x = 1$ but crucially never crosses as Re increases. Similarly, the neutral curve for $k_z = 1$ always has $k_x < 1$, i.e. a long streamwise wavelength is required in this range of Re , and so neither the instabilities with $k_z = 0$ nor $k_z = 1$ are expected to arise in the direct numerical simulations discussed above, with aspect ratio $\alpha = 1$. However, the neutral curves for the instabilities with $k_z > 1$ do intersect $k_x = 1$ (and indeed cross to even higher wavenumbers), suggesting that these instabilities can actually develop within our direct numerical simulations where $\alpha = 1$. The right plot in figure 11 shows the neutral curves on a $B - k_x$ plane, for fixed $Re = 15$, illustrating that increasing B and Re introduces more instabilities with higher values of vertical wavenumber k_z .

5. Exact coherent structures

We can determine if the finite-amplitude states observed in the direct numerical simulations can be connected to the inherently stratified linear instabilities discussed in the previous section by attempting to converge invariant states using a Newton-GMRES-

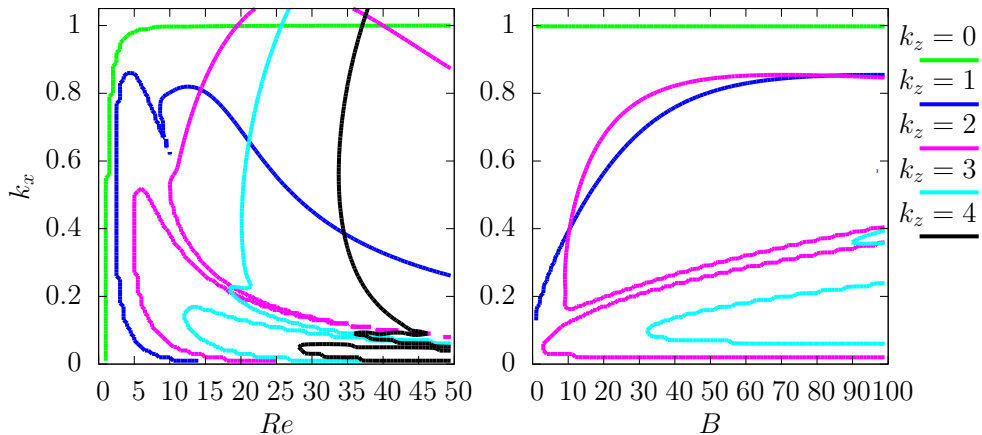


FIGURE 11. Left panel: Neutral stability curves on the $Re - k_x$ plane for modes with vertical wavenumbers $k_z = 0, 1, 2, 3, 4$ in a flow with $B = 50$; Right panel: Neutral stability curves on the $B - k_x$ plane for modes with vertical wavenumbers $k_z = 0, 1, 2, 3, 4$ in a flow with $Re = 15$. Note that the $k_z = 0$ instability has $k_x < 1$ for all Re and B .

hookstep algorithm (Chandler & Kerswell 2013). Successfully converging invariant states and performing arc-length continuation of the solutions in a certain control parameter (for example α , Re , or B) enables us to build a bifurcation diagram for these invariant states.

For reasons of computational efficiency we concentrate initially on unthrottled flows with low Re in relatively long domains with $\alpha < 1$ when attempting to identify invariant states. In such situations, the flow is less ‘unstable’, in the specific sense that relatively simple coherent structures are observed to be approached closely. Therefore we expect our attempts at convergence to meet with more success. Figure 12 shows the results arising from initially converging an unstable invariant state (labelled state (a1)) in a flow with $Re = 8$, $B = 50$ and $\alpha = 0.9$. The initial guess is extracted from a direct numerical simulation by taking a snapshot of the entire state vector when the flow is most quiescent, measured by the dissipation being minimum (in time). This state clearly has one chevron-shaped structure in its streamwise velocity (shown in the top left panel). Due to the assumed periodicity in the vertical direction, this state will naturally form a ‘zig-zag’, as clearly observed in the experiments of Billant & Chomaz (2000a).

By continuing in α along the (dashed) red line, this state is observed to connect, via two bifurcations (via state (a2)) to the state (b) which is the ensuing state arising from the $k_z = 1$ linear instability. Since state (b) arises from a linear instability of the laminar flow, it is marked with a thick line (blue for consistency with the $k_z = 1$ neutral curves in figure 11) and we refer to it as a ‘primary’ state, while we refer to state (a2) as a ‘secondary’ state and plot its continuation with a thin line, arising as it does from a bifurcation from a primary state. We call (a1) a ‘tertiary state’ since it bifurcates from a secondary state and denote it with a dashed line. Note, consistently with the linear stability calculations presented in figure 11, state (b) does not exist in a flow geometry with $\alpha = 1$, but requires $\alpha < 1$. Moreover when increasing α , state (a1),

through a further connecting bifurcation into another secondary state (a3) marked with a thin blue line, is found to connect to the primary state (labelled (c) and marked with a thick green line, once again for consistency with figure 11) arising from the $k_z = 0$ unstratified linear instability of the laminar flow. In other words, the state labelled (c) undergoes its own stratified linear instability (to the state (a3) marked with the light blue line) in much the same fashion as the laminar background flow u_{lam} undergoes the linear instability, ultimately leading to the saturated state (b). The different varieties of chevron shaped states (a1)-(a3) are very similar and only on close inspection is one able to discern the subtle symmetry differences, notably between (a2) and (a3) which are switched by traversing the ‘rung’ of the tertiary state (a1). Note that for the situation described here the values of k_x at which states (b) and (c) bifurcate from the laminar flow can be associated with crossings of the neutral curves in the left panel of figure 11 at $Re = 8$. Furthermore, all states are inherently three-dimensional apart from the states lying along the $k_z = 0$ green curve associated with state (c). In summary we have identified an inherently nonlinear and coherent chevron-shaped structure, which we refer to as state (a), which is highly reminiscent of the finite amplitude structures observed experimentally by Billant and Chomaz. Crucially, we establish that the chevron-shaped structure arises from a **secondary** bifurcation away from the nonlinear state associated with the primary instability, and should not be thought of as the straightforward finite amplitude manifestation of the primary instability consistently with the numerically-based observations of Deloncle *et al.* (2008) that the zig-zag instability does not ‘saturate’, at least for the instability with $k_z = 1$ within our flow domain.

The states shown in figure 12 arise from the $k_z = 0$ and $k_z = 1$ primary instabilities of the laminar base flow, and so are associated with flow geometries with relatively long domains with α strictly less than one (though in some cases quite close to one). However, this is not a necessary restriction. Figure 13 shows the analogous situation for states bifurcating from the $k_z = 0$ linear instability (once again plotted with a thick green line for consistency with the neutral curves plotted in figure 11) and from the $k_z = 2$ linear instability (plotted with a magenta line, also consistently with figure 11). Here, the nonlinear coherent structure is initially found from a guess given by a snapshot of the state vector from a direct numerical simulation with somewhat larger $Re = 15$ with the same $B = 50$ and $\alpha = 0.9$ initially. Here, the nonlinear coherent structure (denoted state (C)) has two chevron-shaped inclined shear layers, as shown in the upper rightmost panel of figure 13, and once again is reminiscent of finite amplitude ‘zig-zag’ structures.

Perhaps unsurprisingly, through continuation (plotted with a thin blue line in the figure) this state is once again found to be ‘secondary’, in that it attaches through bifurcations both to the primary state (shown in figure 13 as state (A), and plotted with a thick magenta line for consistency with figure 11) arising from the linear instability with $k_z = 2$ and the primary state arising from the two-dimensional ($k_z = 0$) linear instability, whose continuation with aspect ratio α is once again plotted with a thick green line. Using continuation, we also identify another secondary state, labelled (B) and plotted with a thin orange line. This state is in some sense lower amplitude, and does not have such strongly inclined layers, although a chevron-shaped structure is still apparent in the streamwise velocity, as shown in the middle upper panel of figure 13. Importantly however, we find that state (B) still persists to $\alpha \geq 1$, notably the local maximum in the solution curve is found at $\alpha \approx 0.997$ and forms a smooth maximum, despite on these axes looking like a sharp cusp.

It should be noted that state (A) does not actually arise in the first, most unstable eigenvalue crossing of the $k_z = 2$ linear instability but rather through a secondary appearance of a new unstable direction of u_{lam} . Equivalently, the associated values of

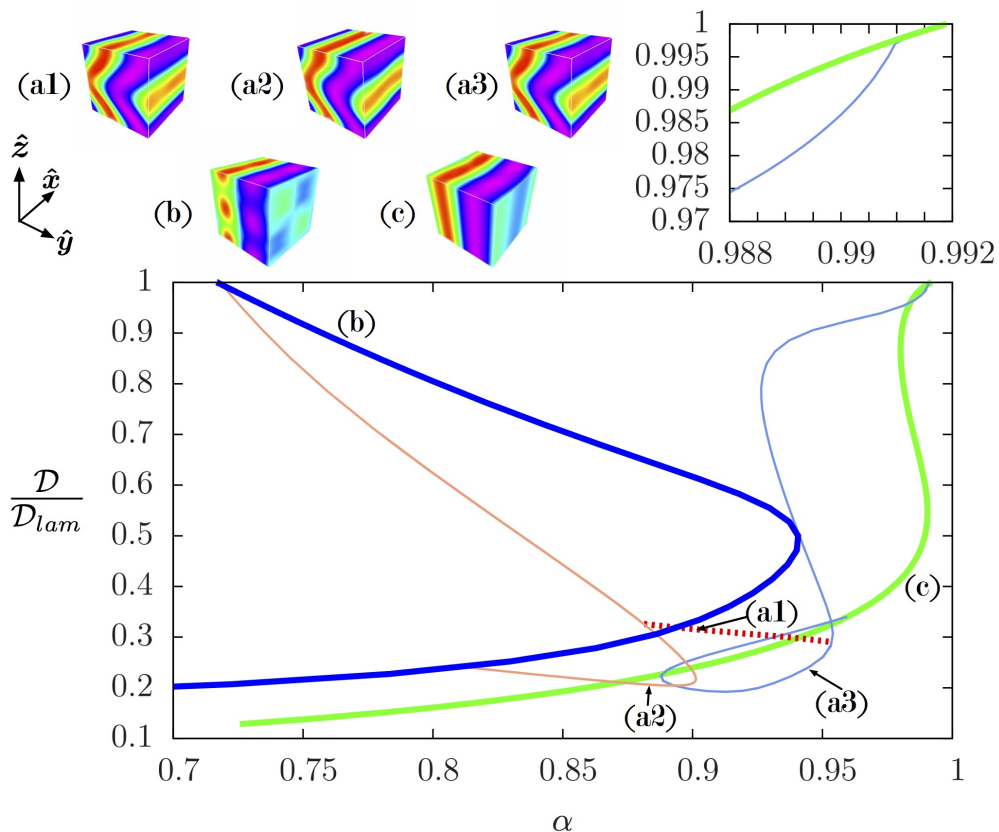


FIGURE 12. Bifurcation diagram showing solution branches for flows with $Re = 8$ and $B = 50$ identified through continuation in α (or equivalently streamwise wavenumber k_x) against scaled total dissipation D/D_{lam} . The spatial structures of streamwise velocity for states (a1)-(c) are shown in the top left. Thick lines are primary states generated by linear instabilities of the laminar velocity profile u_{lam} , (equation (2.11)), thin lines follow secondary states generated by instabilities in of the primary states and dashed lines follow tertiary states, in turn arising from instabilities of the secondary states. The green curve follows the two-dimensional solution state (c) (with $k_z = 0$) connecting to the long-wave homogeneous instability of the laminar base flow. The inset shows a zoom of the bifurcation leading to state (c) and also shows the (secondary) stratified instability from this state leading to the three-dimensional inclined ‘V’-shaped coherent structure (a3) which follows the lighter blue curve as α is continued, and which then through a further tertiary bifurcation (marked with a dashed red line) switches to state (a1). State (a1) follows the red dashed curve in this plane, and in turn attaches to the secondary state (a2) plotted with a thin orange line. State (a2) finally connects to the primary state (b), plotted with a thick dark blue line, which originates from the $k_z = 1$ stratified linear instability of the laminar base flow u_{lam} . Note that the labelling of the curves corresponds to the locations in parameter space for the three-dimensional visualisations plotted above.

k_x do not correspond to the crossing of the main neutral curves plotted in figure 11. We therefore conjecture that further bifurcations at the first appearance (as α increases) will either give rise to yet more coherent nonlinear states, or reconnect to the states discussed here. However, our objective here is not to conduct an exhaustive bifurcation analysis, but rather to identify the origins of the converged chevron-shaped states which

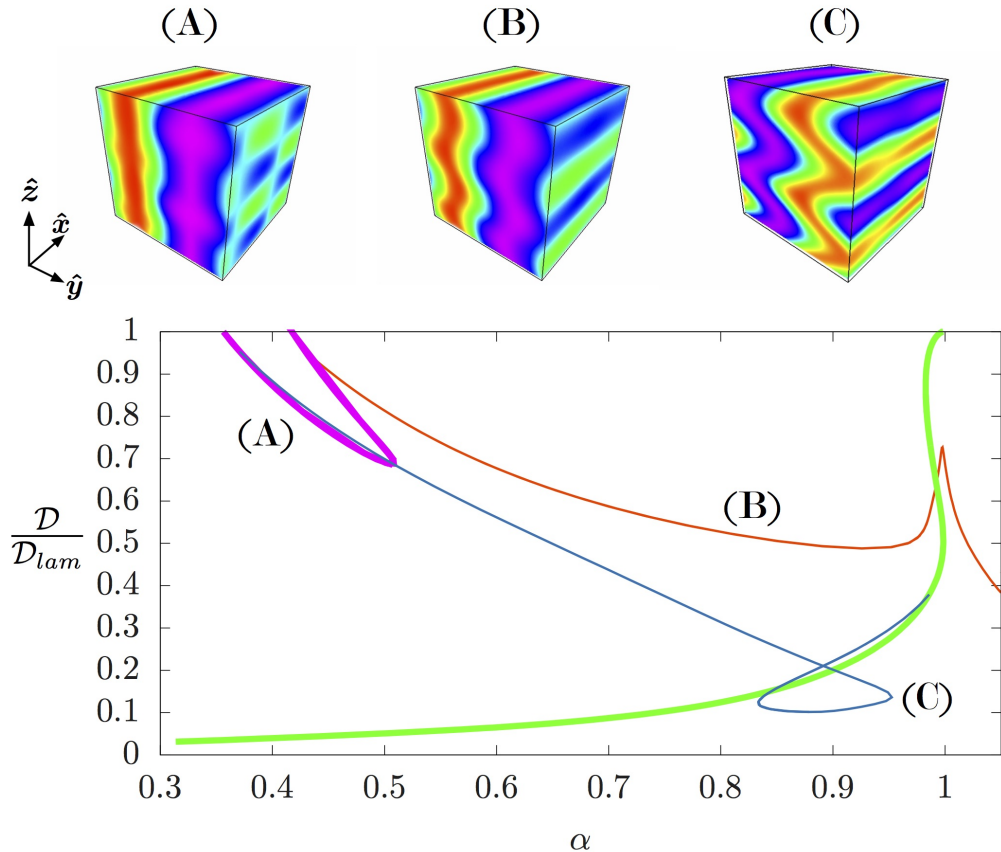


FIGURE 13. Bifurcation diagram showing solution state branches for flows with $Re = 15$ and $B = 50$ identified through continuation in α (or equivalently streamwise wavenumber k_x) against scaled total dissipation D/D_{lam} . The spatial structures of streamwise velocity for states (A)-(C) are shown in the upper panels. As in figure 12 the thick green curve shows the evolution of the primary state arising from the linear instability with $k_z = 0$, while the thick magenta curve shows the evolution of primary state (A), arising from the $k_z = 2$ linear instability of the laminar base flow u_{lam} . The thin orange line shows the evolution of the secondary state (B) and the thin blue line shows the evolution of the secondary state (C), both generated by instabilities of the primary state (A). State (C) also attaches back to the primary state with $k_z = 0$. Labels are placed adjacent to where the three-dimensional visualisations are made in parameter space.

are of interest due to their clear similarity to the previously reported zig-zag structures. Practically, we have also demonstrated the utility of continuation in α as it appears to demonstrate conveniently the bifurcation structure of the various solution states.

In figure 14, we show how the properties (in particular the streamwise velocity structures) of the state (C) change under continuation in the stratification parameter B for α fixed at its original value of 0.9 and $Re = 15$. After some turning points, the curve traced by the solution state closes in on itself. Although it is at least plausible that continuation in B might lead to some smooth variation of the shear inclination as B increases, it is actually apparent that the increasing vertical structure observed in the numerical simulations arises due to the generation through instability of a family of new

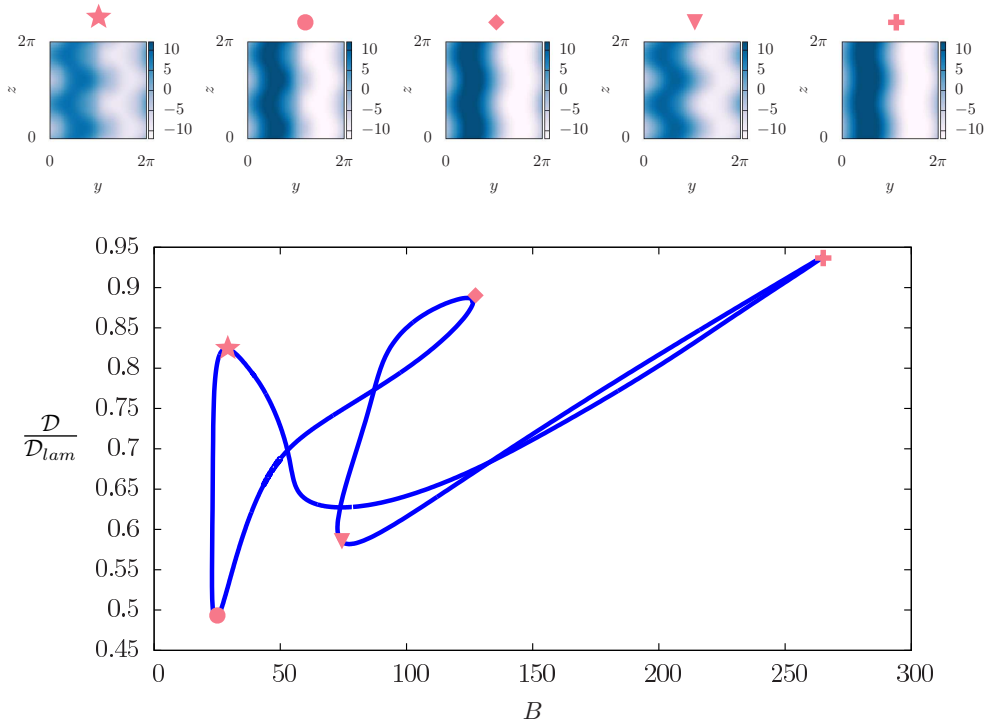


FIGURE 14. Bifurcation diagram showing solution state branch (C) from figure 13 continued in B against normalised total dissipation D/D_{lam} for flows at fixed $\alpha = 0.9$ and $Re = 15$. Visualisations of the streamwise velocity in the $y - z$ mid-plane at $(x = \pi)$ at various labelled locations on the curve are shown in the upper panels. Note that at large B the solution curve bends back upon itself to close the loop.

invariant solution states. It is somewhat surprising that given the complicated behaviour of the solution state curve there is such little variation in the qualitative shape of the flow state, as visualised in figure 14 by the streamwise velocity structure in a $y - z$ midplane at $x = \pi$. Indeed, the direct numerical simulations show that these coherent structure states are subject to additional pattern forming instabilities, generically leading to localisation of the shear in the z -direction and therefore turbulent motions. Typical dynamical behaviour is shown in figure 15 where three-dimensional visualisations of the streamwise velocity u are shown for the extremely strongly stratified and throttled simulation D5 (with $B = 2000$) from table 1. How such localisation comes about is a question for future research, but we note in passing, that although the notional value of Re_B for this simulation is quite low, still the shear instability and layered flow structures bear more than a passing qualitative similarity to those shown in the vigorously turbulent and anisotropic simulation D9.6 of Brethouwer *et al.* (2007) (see in particular their figure 5a).

6. Discussion

In this paper we have attempted to lay out the mechanisms by which the density field is spontaneously arranged into sustained layers by stratified turbulence driven with a horizontal shear. The key step is that we have been able to connect the coherent

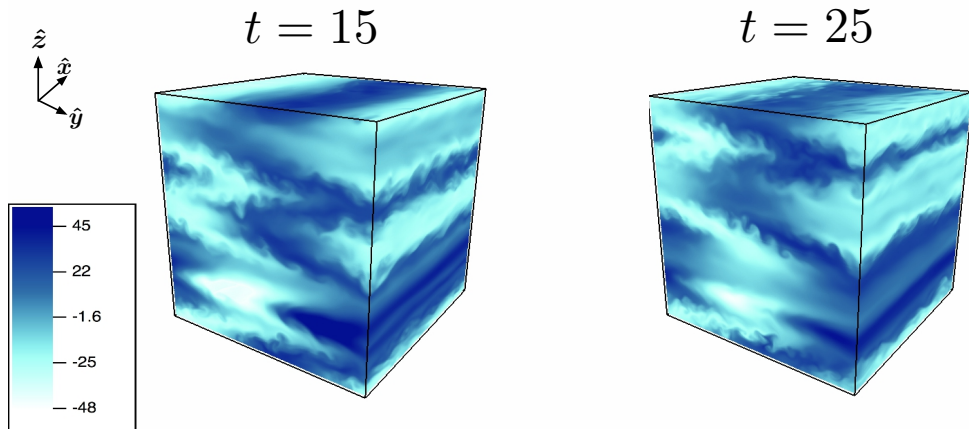


FIGURE 15. Snapshots of streamwise velocity, u , for simulation D5 ($Re = 50$, $D_0 = 250$, $B = 2000$) showing the localisation in the vertical of the coherent structures leading to inherently anisotropic and layered turbulent motions.

structures, observed to organise the mean flow of the turbulence into inclined shear layers, to the stratified linear instabilities of the basic horizontally varying and vertically uniform velocity profile. This is achieved by obtaining, directly from the turbulent numerical simulations, various nonlinear coherent structures as exact, yet unstable, steady states. Specifically, we have found two steady states which are striking representations of the mean flows observed during the turbulence, one state having a single vertical layer and the other state having two layers. By constructing a bifurcation diagram using arc-length continuation in flow parameters, both are found to originate from a sequence of instabilities, the principal or primary of which is a stratified linear instability of the base flow.

We expect the scenario outlined above to be quite general. The linear instability reported here is clearly closely related to the three-dimensional stratified instabilities identified by Billant & Chomaz (2000*c*) for dipoles, and Deloncle *et al.* (2007) for hyperbolic tangent shear layers and Bickley jets. Importantly, we have for the first time identified a family of nonlinear *steady* states which do indeed manifest a chevron-shaped or zig-zag vertical structure, very reminiscent of previously observed finite amplitude structures for a vortex dipole (Billant & Chomaz 2000*a,b*). Turbulence forced with these other profiles may be expected to behave similarly, being organised about unstable steady states with vertically inclined shear layers. How such structures behave as the imposed horizontal shear becomes progressively more localised in space is an interesting and relevant research problem.

The effect of inclination of initial shear relative to the background stratification has been considered in the freely decaying case by Jacobitz & Sarkar (1998). It was found that even a small inclination angle is sufficient to increase turbulent production significantly. The effect of inclination angle on the linear instability of a Bickley jet was considered by Candelier *et al.* (2011), where growth rates are found to be proportional to the sine of the angle. We therefore conjecture that a body-forced inclined shear will generate projected versions of the coherent structures discovered here, eventually vanishing as the shear approaches being purely vertical.

One open question is how precisely the nonlinear solutions obtained correspond to

episodes in the direct numerical simulations at other parameter values, in particular at higher values of the Reynolds number. We do not address this question here, as our principal aim is to demonstrate that flow *structures* of interest can not only be located but also their source (through an identifiable sequence of instabilities and bifurcations) can be determined. It is reasonable to expect that, given sufficient numerical resources, corresponding states at a desired point in parameter space could also be found and we conjecture that a similar picture will emerge there. However it is also plausible that the coherent structures observed in one part of parameter space are mere shadows of solutions existing in a nearby region of parameter space, and therefore solution efforts there would fail to converge, for example at $\alpha = 1$, which appears to be inaccessible to most of the solution state curves described here.

Significantly, the secondary and tertiary instabilities of the exact states we have identified support turbulence which rearranges the density field into well-defined mixed regions and interfaces which are sustained for long times. This aspect, and the mixing properties of this flow will be the subject of a subsequent paper. A fundamental question in stratified turbulence has been how, or indeed if, a stably stratified buoyancy field becomes organised into layers with mixed regions and strong gradients, in particular how the vertical length scales of such layers might be set. Here we have shown, for the first time, a robust connection extending all the way from the linear theory for instability from a simple laminar state, to the nonlinear saturated layered state which is actually observed in the turbulence. As such it places the proposed scaling for the layer depth $l_v \sim U/N$ (in terms of a characteristic velocity scale U and the buoyancy frequency N) on a much stronger foundation. The conventional but formally unjustified assumption that linear theory can explain some aspect of a highly nonlinear turbulent flow is actually here given some justification. However, it is still unclear how the basin or basins of attraction for the turbulence are continuously deformed toward the observed more layered configurations in phase space as the stratification is increased and how this relates to the appearance of the new unstable invariant manifolds (generated via the instabilities) about which the turbulence organises.

REFERENCES

- ARNOLD, V I & MESHALKIN, L D 1960 Seminar led by AN Kolmogorov on selected problems of analysis (1958-1959). *Usp. Mat. Nauk* **15** (247), 20–24.
- AUGIER, PIERRE, BILLANT, PAUL & CHOMAZ, JEAN-MARC 2015 Stratified turbulence forced with columnar dipoles: numerical study. *Journal of Fluid Mechanics* **769**, 403–443.
- BALMFORTH, N. J., LLEWELLYN SMITH, S. G. & YOUNG, W. R. 1998 Dynamics of interfaces and layers in a stratified turbulent fluid. *Journal of Fluid Mechanics* **355**, 329–358.
- BALMFORTH, NEIL J & YOUNG, YUAN-NAN 2002 Stratified Kolmogorov flow. *Journal of Fluid Mechanics* **450**, 131–168.
- BALMFORTH, NEIL J & YOUNG, YUAN-NAN 2005 Stratified Kolmogorov flow. Part 2. *Journal of Fluid Mechanics* **528** (1), 23–42.
- BARENBLATT, G. I., BERTSCH, M., PASSO, R. DAL, PROSTOKISHIN, V. M. & UGHI, M. 1993 A mathematical model of turbulent heat and mass transfer in stably stratified shear flow. *J. Fluid Mech.* **253**, 341–358.
- BASAK, S & SARKAR, S 2006 Dynamics of a stratified shear layer with horizontal shear. *Journal of Fluid Mechanics* **568**, 19–36.
- BILLANT, PAUL & CHOMAZ, JEAN-MARC 2000a Experimental evidence for a new instability of a vertical columnar vortex pair in a strongly stratified fluid. *Journal of Fluid Mechanics* **418**, 167–188.
- BILLANT, P & CHOMAZ, J M 2000b Theoretical analysis of the zigzag instability of a vertical columnar vortex pair in a strongly stratified fluid. *Journal of Fluid Mechanics* **419**, 29–63.

- BILLANT, P & CHOMAZ, J M 2000c Three-dimensional stability of a vertical columnar vortex pair in a stratified fluid. *Journal of Fluid Mechanics* **419**, 65–91.
- BILLANT, PAUL & CHOMAZ, JEAN-MARC 2001 Self-similarity of strongly stratified inviscid flows. *Physics of Fluids* **13** (6), 1645.
- BRETHOUWER, G., BILLANT, P., LINDBORG, E. & CHOMAZ, J.-M. 2007 Scaling analysis and simulation of strongly stratified turbulent flows. *J. Fluid Mech.* **585**, 343–368.
- CANDELIER, JULIEN, LE DIZÈS, STÉPHANE & MILLET, CHRISTOPHE 2011 Shear instability in a stratified fluid when shear and stratification are not aligned. *Journal of Fluid Mechanics* **685**, 191–201.
- CHANDLER, GARY J & KERSWELL, RICH R 2013 Invariant recurrent solutions embedded in a turbulent two-dimensional Kolmogorov flow. *Journal of Fluid Mechanics* **722**, 554–595.
- CHUNG, D & MATHEOU, G 2012 Direct numerical simulation of stationary homogeneous stratified sheared turbulence. *Journal of Fluid Mechanics* **696**, 434–467.
- CVITANOVIĆ, P & GIBSON, J F 2010 Geometry of the turbulence in wall-bounded shear flows: periodic orbits. *Physica Scripta* **142**, 4007.
- DELONCLE, AXEL, BILLANT, PAUL & CHOMAZ, JEAN-MARC 2008 Nonlinear evolution of the zigzag instability in stratified fluids: a shortcut on the route to dissipation. *Journal of Fluid Mechanics* **599**, 229–239.
- DELONCLE, AXEL, CHOMAZ, JEAN-MARC & BILLANT, PAUL 2007 Three-dimensional stability of a horizontally sheared flow in a stably stratified fluid. *Journal of Fluid Mechanics* **570**, 297–305.
- EDEN, CARSTEN & DENGLER, MARCUS 2008 Stacked jets in the deep equatorial Atlantic Ocean. *Journal of Geophysical Research* **113** (C4), C04003–12.
- FALDER, MATTHEW, WHITE, N J & CAULFIELD, C P 2016 Seismic Imaging of Rapid Onset of Stratified Turbulence in the South Atlantic Ocean*. *Journal of Physical Oceanography* **46** (4), 1023–1044.
- GARAUD, PASCALE, GALLET, BASILE & BISCHOFF, TOBIAS 2015 The stability of stratified spatially periodic shear flows at low Péclet number. *Physics of Fluids* **27** (8), 084104–22.
- HOLFORD, JOANNE M & LINDEN, P F 1999a The development of layers in a stratified fluid. In *Mixing and dispersion in stably stratified flows (Dundee, 1996)*, pp. 165–179. Oxford Univ. Press, New York.
- HOLFORD, JOANNE M & LINDEN, P F 1999b Turbulent mixing in a stratified fluid. *Dynamics of Atmospheres and Oceans* **30** (2), 173–198.
- HUA, B L, MOORE, D W & LEGENTIL, S 1997 Inertial nonlinear equilibration of equatorial flows. *Journal of Fluid Mechanics* **331**, 345–371.
- JACOBITZ, FRANK G & SARKAR, SUTANU 1998 The effect of nonvertical shear on turbulence in a stably stratified medium. *Physics of Fluids* **10** (5), 1158–12.
- KAWAHARA, GENTA & KIDA, SHIGEO 2001 Periodic motion embedded in plane Couette turbulence: regeneration cycle and burst. *Journal of Fluid Mechanics* **449**, 291.
- KAWAHARA, GENTA, UHLMANN, MARKUS & VAN VEEN, LENNAERT 2012 The Significance of Simple Invariant Solutions in Turbulent Flows. *Annual Review of Fluid Mechanics* **44** (1), 203–225.
- KERSWELL, R R & TUTTY, O R 2007 Recurrence of travelling waves in transitional pipe flow. *Journal of Fluid Mechanics* **584**, 69–102.
- KREILOS, TOBIAS & ECKHARDT, BRUNO 2012 Periodic orbits near onset of chaos in plane Couette flow. *Chaos: An Interdisciplinary Journal of Nonlinear Science* **22** (4), 047505.
- LECLERCQ, COLIN, PARTRIDGE, JAMIE L, AUGIER, PIERRE, CAULFIELD, COLM-CILLE P, DALZIEL, STUART B & LINDEN, PAUL F 2016 Nonlinear waves in stratified Taylor–Couette flow. Part 1. Layer formation. *arXiv.org* , arXiv: 1609.02885.
- LINDBORG, ERIK 2006 The energy cascade in a strongly stratified fluid. *Journal of Fluid Mechanics* **550** (-1), 207–242.
- LUCAS, DAN & KERSWELL, RICH 2014 Spatiotemporal dynamics in two-dimensional Kolmogorov flow over large domains. *Journal of Fluid Mechanics* **750**, 518–554.
- LUCAS, DAN & KERSWELL, RICH 2016 Sustaining processes from recurrent flows in body-forced turbulence. *arXiv.org* p. arXiv:1611.04829, arXiv: 1611.04829.
- LUCAS, DAN & KERSWELL, RICH R 2015 Recurrent flow analysis in spatiotemporally chaotic 2-dimensional Kolmogorov flow. *Physics of Fluids* **27** (4), 045106–27.

- MAFFIOLI, A., BRETHOUWER, G. & LINDBORG, E. 2016 Mixing efficiency in stratified turbulence. *J. Fluid Mech.* **794**, R3 12 pages.
- MARCHIORO, C 1986 An example of absence of turbulence for any Reynolds number. *Communications in Mathematical Physics* **105** (1), 99–106.
- MASHAYEK, A., CAULFIELD, C. P. & PELTIER, W. R. 2013 Time-dependent, non-monotonic mixing in stratified turbulent shear flows: implications for oceanographic estimates of buoyancy flux. *J. Fluid Mech.* **736**, 570–593.
- OGLETHORPE, R L F, CAULFIELD, C P & WOODS, ANDREW W 2013 Spontaneous layering in stratified turbulent Taylor–Couette flow. *Journal of Fluid Mechanics* **721**, R3–12.
- PARK, Y. G., WHITEHEAD, J. A. & GNANADESKIAN, A. 1994 Turbulent mixing in stratified fluids: layer formation and energetics. *J. Fluid Mech.* **279**, 279–311.
- PHILLIPS, O M 1972 Turbulence in a strongly stratified fluid—is it unstable? *Deep Sea Research and Oceanographic Abstracts* **19** (1), 79–81.
- PORTWOOD, G. D., DE BRUYN KOPS, S. M., TAYLOR, J. R., SALEHIPOUR, H. & CAULFIELD, C. P. 2016 Robust identification of dynamically distinct regions in stratified turbulence. *J. Fluid Mech.* **807**, R2 14 pages.
- THORPE, S A 2016 Layers and internal waves in uniformly stratified fluids stirred by vertical grids. *Journal of Fluid Mechanics* **793**, 380–413.
- VAN VEEN, LENNAERT & GOTO, SUSUMU 2015 Sub critical transition to turbulence in three-dimensional Kolmogorov flow. *arXiv.org* p. arXiv:1512.02570, arXiv: 1512.02570.
- VAN VEEN, LENNAERT & KAWAHARA, GENTA 2011 Homoclinic Tangle on the Edge of Shear Turbulence. *Physical review letters* **107** (11), 114501.
- VAN VEEN, LENNAERT, KIDA, SHIGEO & KAWAHARA, GENTA 2006 Periodic motion representing isotropic turbulence. *Japan Society of Fluid Mechanics. Fluid Dynamics Research. An International Journal* **38** (1), 19–46.
- VENAILLE, A., GOSTIAUX, L. & SOMMERIA, J. 2016 A statistical mechanics approach to mixing in stratified fluids. *J. Fluid Mech.* **810**, 554–583.
- VENAYAGAMOORTHY, S. K. & KOSEFF, J. R. 2016 On the flux Richardson number in stably stratified turbulence. *J. Fluid Mech.* **798**, R1 10 pages.
- VISWANATH, DIVAKAR 2007 Recurrent motions within plane Couette turbulence. *Journal of Fluid Mechanics* **580**, 339.
- WAITE, MICHAEL L & SMOLARKIEWICZ, PIOTR K 2008 Instability and breakdown of a vertical vortex pair in a strongly stratified fluid. *Journal of Fluid Mechanics* **606**, 1–35.
- VAN DER WALT, STÉFAN, COLBERT, S CHRIS & VAROQUAUX, GAËL 2011 The NumPy Array: A Structure for Efficient Numerical Computation. *Computing in Science & Engineering* **13** (2), 22–30.
- WILLIS, ASHLEY P & SHORT, KIMBERLY Y 2015 Relative periodic orbits form the backbone of turbulent pipe flow. *arXiv.org* (2), arXiv:1504.05825, arXiv: 1504.05825.